Title

HCN channels are a novel therapeutic target for cognitive dysfunction in Neurofibromatosis type 1

Journal

Molecular Psychiatry, 20(11)

ISSN

1359-4184

Authors

Omrani, A
van der Vaart, T
Mientjes, E
et al.

Publication Date

2015-11-01

DOI

10.1038/mp.2015.48

Peer reviewed

HHS Public Access

Author manuscript

Mol Psychiatry. Author manuscript; available in PMC 2017 September 19.

Published in final edited form as:

Mol Psychiatry. 2015 November ; 20(11): 1311–1321. doi:10.1038/mp.2015.48.

HCN channels are a novel therapeutic target for cognitive dysfunction in Neurofibromatosis type 1

A Omrani[1,2,10], **T van der Vaart**[1,2,3], **E Mientjes**[1,2], **GM van Woerden**[1,2], **MR Hojjati**[1,4], **KW Li**[5], **DH Gutmann**[6], **CN Levelt**[7], **AB Smit**[5], **AJ Silva**[8], **SA Kushner**[2,9], and **Y Elgersma**[1,2]

[1]Department of Neuroscience, Erasmus Medical Center, Rotterdam, The Netherlands [2]ENCORE Center for Neurodevelopmental Disorders, Erasmus Medical Center, Rotterdam, The Netherlands [3]Department of Pediatrics, Erasmus Medical Center, Sophia Children's Hospital, Rotterdam, The Netherlands [4]Department of Physiology, Shahrekord University of Medical Sciences, Shahrekord, Iran [5]Department of Molecular and Cellular Neurobiology, CNCR, Neuroscience Campus Amsterdam, VU University, Amsterdam, The Netherlands [6]Department of Neurology, Washington University School of Medicine, St. Louis, MO, USA [7]Department of Molecular Visual Plasticity, Netherlands Institute for Neuroscience, Royal Netherlands Academy of Arts and Sciences (KNAW), Amsterdam, The Netherlands [8]Department of Neurobiology, Brain Research Institute, University of California Los Angeles, Los Angeles, CA, USA [9]Department of Psychiatry, Erasmus Medical Center, Rotterdam, The Netherlands

Abstract

Cognitive impairments are a major clinical feature of the common neurogenetic disease neurofibromatosis type 1 (NF1). Previous studies have demonstrated that increased neuronal inhibition underlies the learning deficits in NF1, however, the molecular mechanism underlying this cell-type specificity has remained unknown. Here, we identify an interneuron-specific attenuation of hyperpolarization-activated cyclic nucleotide-gated (HCN) current as the cause for increased inhibition in *Nf1* mutants. Mechanistically, we demonstrate that HCN1 is a novel NF1-interacting protein for which loss of NF1 results in a concomitant increase of interneuron excitability. Furthermore, the HCN channel agonist lamotrigine rescued the electrophysiological and cognitive deficits in two independent *Nf1* mouse models, thereby establishing the importance of HCN channel dysfunction in NF1. Together, our results provide detailed mechanistic insights

Correspondence: Professor Y Elgersma, Department of Neuroscience, Erasmus Medical Center, Wytemaweg 80, PO Box 2040, CA, Rotterdam 3000, The Netherlands. y.elgersma@eramsusmc.nl.

[10]Present address: Department of Translational Neuroscience, Brain Center Rudolf Magnus, University Medical Center Utrecht, Utrecht, The Netherlands.

CONFLICT OF INTEREST

The authors declare no conflict of interest.

AUTHOR CONTRIBUTIONS

AO conducted electrophysiology experiments, immunohistochemistry and data analysis. YE generated the $Nf1^{9a-/9a-}$ mouse in the laboratory of AJS. TvdV carried out behavioral experiments and data analysis. GvW and EM performed biochemical experiments and immunohistochemistry. MRH contributed to field-potential recordings. KWL conducted proteomics experiments and data analysis. DHG, ABS, CNL and AJS provided critical insight and reagents. AO, SAK and YE designed the study and wrote the manuscript with input from all authors.

Supplementary Information accompanies the paper on the Molecular Psychiatry website (http://www.nature.com/mp)

into the pathophysiology of NF1-associated cognitive defects, and identify a novel target for clinical drug development.

INTRODUCTION

Neurofibromatosis type 1 (NF1, incidence 1:3000) is caused by mutations in the *NF1* gene. The *NF1* gene product, neurofibromin, contains a Ras GTPase-activating protein domain, which serves as a negative regulator of Ras/ERK signaling. The clinical symptoms of NF1 include cutaneous neurofibromas, café-au-lait spots, skinfold freckling and Lisch nodules, as well as cognitive deficits that negatively impact school performance and quality of life.[1,2] Mice with a heterozygous null mutation of the *Nf1* gene ($Nf1^{+/-}$ mice) closely model the cognitive deficits and behavioral difficulties experienced by human NF1 patients, including visual-spatial learning, working memory, attention and motor performance deficits.[3–5]

Previously, it has been shown that the learning deficits of $Nf1^{+/-}$ mice result from hyperactivation of Ras signaling in GABAergic neurons, despite expression of the neurofibromin/Ras in both excitatory and inhibitory neurons.[3,6] The specificity of this phenotype is further surprising, given that it is not recapitulated in other mouse models in which Ras-ERK signaling is upregulated, such as mouse models for Noonan syndrome and Costello syndrome.[7] This suggests that NF1 might also have a Ras-independent function in neurons. Ras-independent targets hold substantial therapeutic potential, as Ras itself is difficult to target, and drugs that interfere with downstream Ras signaling have poor tissue specificity and undesirable side effects, limiting their utility for treating cognitive dysfunction. Moreover, two randomized controlled trials targeting Ras activity in NF1 patients demonstrated no evidence of clinical efficacy.[8,9]

In the present study, we sought to define the mechanisms underlying the cell-type-specific pathophysiology underlying the learning deficits of *Nf1* mice. Given the widespread expression of neurofibromin in neuronal and glial cell types, we focused our efforts on a novel *Nf1* mouse mutant with deletion of the neuron-specific NF1 exon 9a isoform ($Nf1^{9a-/9a}$). Exon 9a is a short 10 amino-acid sequence in the amino-terminal region, the presence of which does not influence the function of the Ras GTPase-activating protein domain.[10] Expression of the exon 9a isoform begins postnatally and is highly abundant in the septum, striatum, cortex and hippocampus.[10–12] We found that $Nf1^{9a-/9a-}$ mice recapitulate the phenotypes observed in the global $Nf1^{+/-}$ mice, including deficits in hippocampal synaptic plasticity and learning, as well as enhanced inhibitory synaptic transmission. Furthermore, we identified the hyperpolarization-activated cyclic nucleotide-gated channel 1 (HCN1) as a neurofibromin-interacting protein. HCN1 belongs to the family of voltage-gated ion channels that mediate an inward cationic current (I_h),[13] which contributes to intrinsic excitability, pacemaker activity and synaptic integration.[14–16] Accordingly, increasing evidence has implicated I_h in activity-dependent plasticity, learning and memory, and epilepsy.[17–21] Furthermore, HCN1 is enriched in cortical and hippocampal parvalbumin-expressing interneurons.[22–26] We now demonstrate attenuation of I_h and subsequent enhancement of excitability in interneurons of *Nf1* mutant mice. Moreover, we show that the attenuation of I_h underlies the increased inhibitory neurotransmission in

$Nf1^{9a-/9a-}$ and $Nf1^{+/-}$ mice, such that increasing HCN current with lamotrigine (LTG) rescues the electrophysiological and learning deficits in both $Nf1^{9a-/9a-}$ and $Nf1^{+/-}$ mice.

MATERIALS AND METHODS

Animals

Experimental mice were obtained by crossing $Nf1^{9a-/9a+}$ mice (in C57BL/6JOlaHsd background) with 129T2/SvEmsJ (Jackson Laboratories, Bar Harbor, ME, USA) by crossing the obtained F1 mutant mice with each other to get homozygous $Nf1^{9a-/9a-}$ mutants and wild-type (WT) littermates in the hybrid B6/129T2 background, comparable to that of previous studies in NF1. Homozygous $Nf1^{9a-/9a-}$ mice were born at the expected Mendelian frequency, and were indistinguishable from WT mice upon examination by an experienced observer. Male $Nf1^{+/-}$ mice (C57BL/6JOlaHsd, >30 generations) were crossed once with WT 129T2/SvEmsJ mice (Jackson Laboratories) to obtain F1 hybrid B6/129T2 heterozygous mutant and WT control mice. $H\text{-}Ras^{G12V}$ mice in C57BL/6JOlaHsd background were obtained by crossing heterozygous $H\text{-}Ras^{G12V}$ mice to yield homozygous $H\text{-}Ras^{G12V}$ mice and WT control mice. For all experiments, we used both male and female mice. All mice were between 8 and 15 weeks of age at the start of the behavioral experiments, housed in groups of 2–4 per cage, on a 12-h light/dark cycle between 0700 and 1900 hours, and fed standard laboratory food *ad libitum*. All included animals were healthy (discomfort score 0). Behavioral experiments were performed between 1200 and 1800 hours. For *ex-vivo* experiments, mice were killed between 0900 and 1200 hours. Experimenters were blind for genotype and treatment. All experiments were approved by the Dutch Ethical Committee and were in accordance with the institutional animal care and use committee guidelines.

Slice electrophysiology

Hippocampal slices were prepared from the brains of 3- to 4-week-old and adult mice using standard techniques. Field excitatory postsynaptic potentials (EPSPs) were evoked in CA3-CA1 synapses and whole-cell patch-clamp recording were performed from hippocampal CA1 pyramidal neurons and interneurons. For interneurons recordings, 0.2% biocytin was included in the intracellular pipette solution for later morphological identification of the recorded cells. Standard protocols were followed for recording and data analysis. For additional information, see Supplementary Materials and Methods.

Morris water maze

The water maze task was performed as previously described.[27] Before performing the water maze task, the mice were handled for a week. For initial characterization of $Nf1^{9a-/9a-}$ mice, training consisted of 4 trials per day, divided in two sessions of two trials with a 1 h interval (Figure 1) or two trials per day for LTG-treated mice. At the start of the first session the mice were placed on the platform for 30 s. Then they were placed in the water at a pseudo-random start position and allowed to find the platform for 60 s. If the mice did not find the platform within 60 s, it was placed onto the platform and allowed to remain on it for 30 s. The platform position remained at the same position during all trials. Spatial memory was assessed with a probe trial given 1–2 h (Figure 1d) or 22–24 h after the last training trial

(Figure 5), when the majority of the mice was able to locate the platform in less than 30 s (after 3 training days for mice in Figure 1d and 5e and after 5 training days for Figure 5d). During probe trials mice were placed on the platform for 30 s, after which the platform was removed from the pool and the mice were placed in the pool at the opposite side of the previous platform position. The mice were then allowed to search for the platform for 60 s. The visible water maze was performed with a new group of mice. After the handling period, mice were trained in the pool to find the escape platform which was flagged with a small cue on the top of the platform. The platform location and the start position were changed on every trial and each mouse received four trials per day for 8 consecutive days. Mice were excluded from further analysis if they showed excessive (>20%) floating (throughout the training or at the probe trial itself), or would not stay on the platform after training day 2. With respect to exclusion criteria, no differences between genotypes were observed (typically 1–2 mice per genotype are excluded).

Rotarod

Motor learning was assessed with the accelerating rotarod (Ugo Basile, Comerio Varese, Italy) as previously described.[5] Each animal was placed on a 3-cm diameter cylinder, accelerated from 4 to 40 r.p.m. for maximum 5 min. All animals were given five trials during one day, with an inter-trial interval of 45 min. The latency time to fall was measured in seconds.

Statistical analysis

All data are reported as means ± s.e.m. Cumulative miniature and spontaneous synaptic currents amplitude and inter-event interval distributions were analyzed for statistical significance using the Kolmogorov–Smirnov test (Mini Analysis), and a conservative critical probability level of $P < 0.01$. All other statistical tests, including *t*-tests and one- or two-way analysis of variance, were performed using a critical probability of $P < 0.05$ and two-sided testing (Prism, GraphPad Software, Inc., La Jolla, CA, USA and SPSS, IBM Corporation, Armonk, NY, USA). *Post hoc* analyses were performed only when an analysis of variance yielded a significant ($P < 0.05$) main effect.

RESULTS

Nf1$^{9a-/9a-}$ mice have impaired spatial learning and synaptic plasticity

We generated a novel *Nf1* mouse model (the homozygous *Nf1*$^{9a-/9a-}$ mutant), in which the neuron-specific NF1 exon 9acontaining isoform is deleted. Reverse transcription-quantitative PCR confirmed the total absence of Nf1 exon 9a-containing mRNA in *Nf1*$^{9a-/9a-}$ mice (Figure 1a and Supplementary Figure 1). Consistent with the relatively high abundance of this neuronal isoform in the hippocampus, total *Nf1* mRNA was reduced by 36 ± 7% ($n = 9$, Figure 1b), with concomitant reduction of total neurofibromin protein (a reduction of 39 ± 2% in the hippocampus, $n = 11$; Figures 1b and c). *Nf1*$^{9a-/9a-}$ mice were born at the expected Mendelian frequency and appeared healthy. Notably, and in contrast to *Nf1*$^{+/-}$ mice,[5] *Nf1*$^{9a-/9a-}$ mice have no detectable motor impairments (Supplementary Figure 2a).

Visual-spatial problems are among the most frequent cognitive deficits observed in NF1 patients.[28] Therefore, $Nf1^{9a-/9a-}$ mice were tested in the Morris water maze task previously demonstrated to be impaired in $Nf1^{+/-}$ mice.[3,4,29] Indeed, $Nf1^{9a-/9a-}$ mice utilized an exclusively non-spatial search strategy and showed no preference for the target quadrant (Figure 1d). Analogous to $Nf1^{+/-}$ mice, this deficit was not the result of decreased motivation or impaired swimming performance, given that $Nf1^{9a-/9a-}$ mice showed no changes in swimming speed, thigmotaxis or the ability to learn the visible platform version of the water maze (Supplementary Figures 2b and e). These results indicate that intact expression of the neuron-specific Nf1 exon 9a isoform is required for normal spatial learning.

To determine whether the spatial learning impairments of $Nf1^{9a-/9a-}$ mutants are associated with changes in synaptic function, we recorded field excitatory postsynaptic potentials from hippocampal Schaffer collateral-CA1 synapses. No significant differences were found between $Nf1^{9a-/9a-}$ and WT mice in baseline synaptic transmission or paired-pulse ratio (Supplementary Figures 2f,g). Long-term potentiation (LTP) was induced by theta burst stimulation (TBS), a form of stimulation that mimics endogenous hippocampal activity during spatial exploration.[30] In contrast to their WT littermates, $Nf1^{9a-/9a-}$ mice showed a significant deficit in TBS-induced LTP (Figure 1e). Consistent with the sensitivity of TBS-induced LTP to changes in GABAergic inhibition,[31] LTP was normal when induced using a high-frequency stimulation (HFS) protocol (Figure 1f). Furthermore, partial block of inhibitory neurotransmission with picrotoxin (10 μM) fully restored TBS-induced LTP in $Nf1^{9a-/9a-}$ mice (Figure 1g). Given the similarities to $Nf1^{+/-}$ mice,[3,6] we reasoned that the neuron-specific $Nf1^{9a-/9a-}$ mice might share a similar GABAergic mechanism underlying the learning deficits.

$Nf1^{9a-/9a-}$ mice show increased inhibition

To further characterize changes in inhibition, we measured evoked monosynaptic inhibitory postsynaptic potentials using whole-cell recordings from CA1 pyramidal neurons. Notably, inhibitory postsynaptic potential amplitude was bigger at higher stimulus levels in $Nf1^{9a-/9a-}$ mice, whereas paired-pulse ratio was reduced, suggesting a change in presynaptic GABA release (Figure 2a). Spontaneous miniature inhibitory postsynaptic currents recorded from $Nf1^{9a-/9a-}$ and WT mice showed no significant differences in normal artificial cerebrospinal fluid. However, enhancing synaptic GABA release by depolarizing synaptic terminals with high extracellular potassium (12.5 mM) resulted in a significantly increased miniature inhibitory postsynaptic current frequency (but not amplitude) in $Nf1^{9a-/9a-}$ neurons compared with WT controls (Figures 2b and c). This phenotype is similar to $Nf1^{+/-}$ mice[6] and consistent with the observed increase of evoked inhibitory postsynaptic potential amplitude at higher stimulus intensities. Taken together, these results indicate that enhanced GABA release underlies the increased inhibition in $Nf1^{9a-/9a-}$ mutant mice.

We subsequently characterized excitatory synaptic transmission in CA1 pyramidal cells. Consistent with a selective modulation of inhibition, no significant differences were observed for evoked excitatory postsynaptic potentials (EPSPs) or paired-pulse ratio (Figure 2d). In addition, the frequency and amplitude of miniature excitatory postsynaptic currents

were normal, recorded in both standard and high extracellular potassium (Figures 2e and f). Taken together, our results demonstrate that the synaptic abnormalities seen in $Nf1^{9a-/9a-}$ mice are specific for inhibitory neurons, and closely resemble those of $Nf1^{+/-}$ mice. This finding in $Nf1^{9a-/9a-}$ mice is an important and independent replication of the previously described phenotype of $Nf1^{+/-}$ mice,[6] emphasizing the importance of GABAergic dysfunction in the pathophysiology of NF1.

HCN1 co-immunoprecipitates and co-localizes with NF1

Previous studies have identified NF1-interacting proteins, both within and beyond the Ras signaling pathway. Therefore, we sought to utilize the neuron-specific exon 9a mutants, to perform an unbiased and focused comparative proteomics approach for uniquely identifying binding partners of NF1 specifically in neurons. Lysates prepared from WT and $Nf1^{9a-/9a-}$ mice were used for co-immunoprecipitation (co-IP) with anti-neurofibromin antibody followed by mass spectrometry for protein identification. In addition to the previously identified neurofibromin-interacting proteins, tubulin and actin,[32,33] we identified HCN1 as a novel putative neurofibromin-interacting protein (Supplementary Table 1). HCN1 is a particularly compelling candidate, given its well-established role in regulating neuronal excitability. Moreover, HCN1 has been previously found to have prominent enrichment in cortical and hippocampal GABAergic neurons, in particular parvalbumin-expressing interneurons.[22–26] The proteomics findings were confirmed by western blot analysis of immunoprecipitated proteins from $Nf1^{9a-/9a-}$ and WT lysates (Figure 3a). Although there was a trend toward reduced amounts of co-precipitated HCN in the $Nf1^{9a-/9a-}$ mutants, this difference was not significant. In addition to HCN1, HCN2 and the HCN-interacting protein TRIP8b were detected in anti-neurofibromin immunoprecipitates. However, these proteins were not observed when brains of $Hcn1^{-/-}$ mice were used for the co-IP. Therefore, we conclude that both HCN2 and TRIP8b were precipitated through their (known) interaction with HCN1, rather than through direct binding to neurofibromin. Moreover, we observed no difference in the total level of HCN1, HCN2 or TRIP8b when we compared hippocampal lysates of WT and $Nf1^{9a-/9a-}$ mice (Figure 3a).

To further investigate the interaction between HCN1 and NF1, we performed heterologous expression studies in HEK293T cells. Cells were co-transfected with a plasmid expressing the N-terminal half of NF1 (with or without exon 9a) fused to GFP (NF1-GFP), together with a plasmid-expressing HCN1. Lysates were subsequently used for co-IP with the anti-HCN1 antibody. NF1-GFP was successfully identified in the co-IP with the HCN1 antibody. However, consistent with the co-IP results in hippocampal lysates, this interaction does not depend on the presence of exon 9a (Figure 3b). Taken together, these results indicate that NF1 interacts with HCN1 through its N-terminal domain, but the N-terminal exon 9a is not required for this interaction.

Cell-type-specific reduction of HCN current in $Nf1^{9a-/9a-}$ mice

To examine the functional impact of the interaction between NF1 and HCN1 on hyperpolarization-activated cation current (I_h), we measured I_h in both inhibitory and excitatory neurons in the hippocampal CA1 area. We were particularly interested in fast-spiking parvalbumin (PV)-expressing neurons, given that expression of HCN1[23,24] is highly

enriched in PV neurons of the hippocampus. Immunohistochemistry of hippocampal slices confirmed the presence of both HCN1 and NF1 in PV neurons (Figures 3c and d). We recorded from interneurons with somata located at the border of stratum pyramidale and oriens. Cells were identified as fast-spiking PV neurons based on electrophysiological characteristics and *post-hoc* immunoreactivity for PV (see Supplementary Materials and Methods and Figure 4a). Hyperpolarizing steps from a holding potential of −50 mV resulted in slowly activating inward currents (Figure 4b). I_h was pharmacologically isolated by subtracting current traces before and after application of the HCN antagonist ZD7288 (30 μM). Steady-state current–voltage (*I–V*) relation showed smaller I_h at more hyperpolarized potentials in $Nf1^{9a-/9a-}$ mice (Figure 4c). The activation curve of I_h was obtained by plotting the normalized tail current amplitude as a function of the voltage step. Fits of the activation curve with a Boltzmann function yielded a hyperpolarizing shift of 7 mV in the half-activation potential ($V_{1/2}$) in $Nf1^{9a-/9a-}$ mice (−88.4 ± 1.9 mV, $n = 10$) compared with their WT littermates (−81.2 ± 2.0 mV, $n = 7$, $P < 0.01$; Figure 4d). The shift in $V_{1/2}$ influenced neither the slope of activation curve (WT: 11.4 ± 1.3 mV, $P = 0.5$; $Nf1^{9a-/9a-}$: 11.2 ± 1.4 mV) nor the kinetics of I_h (Supplementary Figure 3).

As HCN1 expression is not restricted to PV interneurons, we tested if the alterations in I_h are also observed in excitatory neurons. Hence, we recorded I_h in CA1 pyramidal neurons. Importantly, no significant differences were observed in either the current–voltage relationship or in the voltage dependence of I_h between pyramidal neurons from $Nf1^{9a-/9a-}$ and WT littermates (Figures 4f and g). Both $V_{1/2}$ and the slope factor were also unchanged in pyramidal neurons (−85.9 ± 1.8 and 13.8 ± 0.8 mV ($n = 10$) for $Nf1^{9a-/9a-}$; −83.9 ± 1.1 mV and 14.3 ± 0.6 mV ($n = 9$) for WT, respectively). Furthermore, the I_h kinetics remained intact (Supplementary Figure 3). Taken together, these findings suggest that $Nf1^{9a-/9a-}$ mice have a selective reduction of I_h in GABAergic interneurons.

Several studies have shown that decreases in I_h result in neuronal hyperexcitability.[16,17,20,34] Therefore, we examined whether neuronal excitability was altered in PV neurons of $Nf1^{9a-/9a-}$ mutants. Current-clamp recordings revealed that PV neurons of $Nf1^{9a-/9a-}$ mice had a significantly hyperpolarized resting membrane potential (−64.1 ± 0.7 mV, $n = 17$ vs −60.6 ± 0.7 mV, $n = 12$; $P < 0.005$) and a higher input resistance (279 ± 19 MΩ, $n = 15$ vs 235 ± 14 MΩ, $n = 16$, $P < 0.05$). Next, we measured the excitability of PV neurons from $Nf1^{9a-/9a-}$ and WT mice. Despite having a hyperpolarized resting membrane potential, PV neurons from $Nf1^{9a-/9a-}$ mice produced a significantly greater number of action potentials (Figure 4e). Importantly, the increase of action potential firing is not likely caused by alterations in sodium channels as there was no significant change in action potential threshold. Accordingly, other action potential parameters including peak amplitude, half-width and rise time were unchanged (Supplementary Table 2).

Given the observed differences in the intrinsic membrane properties of PV neurons from $Nf1^{9a-/9a-}$ mice, we also sought to quantify these parameters for CA1 pyramidal neurons. In contrast to PV neurons, neither the resting membrane potential ($Nf1^{9a-/9a-}$: −68.1 ± 0.9 mV, $n = 17$ and WT: −66.5 ± 0.8 mV, $n = 23$; $P = 0.2$) nor the input resistance ($Nf1^{9a-/9a-}$: 116 ± 4.5 MΩ, $n = 18$ and WT: 118 ± 4.5 MΩ, $n = 14$; $P = 0.8$) was altered in pyramidal neurons. In addition, the relative sag amplitude was similar between genotypes (WT: 1.2 ± 0.03 and

Nf1$^{9a-/9a-}$: 1.1 ± 0.02, $P = 0.3$), as well as the action potential threshold, peak amplitude, half-width and rise time (Supplementary Table 2). Moreover, the excitability of pyramidal neurons was also normal in *Nf1*$^{9a-/9a-}$ mice (Figure 4h), confirming the highly selective impact of NF1 function in GABAergic interneurons.

Next, we investigated whether the novel findings observed in the *Nf1*$^{9a-/9a-}$ mice also apply to the *Nf1*$^{+/-}$ mouse model of NF1.[3,6] Similar to that in *Nf1*$^{9a-/9a-}$ mice, I_h was smaller in *Nf1*$^{+/-}$ PV neurons, and its activation was shifted toward more hyperpolarized potentials (Supplementary Figures 4a and b). The half-activation potential for I_h in *Nf1*$^{+/-}$ PV neurons was −89.7 ± 1.7 mV ($n = 7$) compared with −84.7 ± 1.1 mV ($n = 7$) from WT littermates $P < 0.01$. In addition, the average maximal tail current amplitude was substantially lower in PV neurons of *Nf1*$^{+/-}$ mice (−65 ± 11 pA) compared with WT littermates (−96 ± 12 pA; $P < 0.05$), whereas the slope of activation remained unchanged (*Nf1*$^{+/-}$: 10.4 ± 0.8 mV, WT: 9.9 ± 0.7 mV; $P = 0.30$). Furthermore, as observed for *Nf1*$^{9a-/9a-}$ mice, the resting membrane potential of *Nf1*$^{+/-}$ PV neurons was hyperpolarized (−65.1 ± 1.1 mV, $n = 14$ vs −61.8 ± 0.8 mV, $n = 9$; $P < 0.05$) and the input resistance was elevated (289 ± 15.0 MΩ, $n = 16$ vs 258 ± 9.5 MΩ, $n = 18$; $P < 0.05$). In addition, and consistent with a significant downregulation of I_h, *Nf1*$^{+/-}$ PV neurons showed increased excitability (Supplementary Figure 4c), without any significant differences in the characteristics of the action potential voltage waveform or threshold (Supplementary Table 3). Finally, and in contrast to the changes observed in PV neurons, *Nf1*$^{+/-}$ pyramidal neurons showed no alterations in I_h amplitude, voltage-dependent activation or intrinsic excitability (Supplementary Figures 4d–f).

To determine whether other subtypes of interneurons also have attenuation of I_h, we recorded from stratum oriens-alveolus (OA) interneurons of the hippocampal CA1 region, a major class of dendritically targeting interneurons.[14] Similar to our findings in PV neurons, both *Nf1*$^{9a-/9a-}$ and *Nf1*$^{+/-}$ mice exhibited a reduction of I_h in OA interneurons, including the activation being shifted toward more hyperpolarized potentials (Supplementary Figures 5a and b). The half-activation potential for I_h in *Nf1*$^{9a-/9a-}$ OA interneurons was −89.4 ± 1.4 mV ($n = 6$) compared with −81.5 ± 2.9 mV ($n = 5$) from WT littermates ($P < 0.05$). The half-activation potential for I_h in *Nf1*$^{+/-}$ OA interneurons was −87.4 ± 0.9 mV ($n = 10$), compared with −83.1 ± 1.7 mV ($n = 7$) from WT littermates ($P < 0.05$). Furthermore, and consistent with a significant down-regulation of I_h, *Nf1*$^{9a-/9a-}$ and *Nf1*$^{+/-}$ OA interneurons were more excitable than their WT controls (Supplementary Figure 5c).

Previous studies have demonstrated that Nf1$^{+/-}$ mice have increased GABAergic transmission across multiple brain regions.[35,36] Therefore, we sought to examine whether the attenuation of I_h in *Nf1* mice is restricted to hippocampal interneurons, or is also evident in other brain regions. We recorded from layer 1 (L1) interneurons of the visual cortex in *Nf1*$^{+/-}$ mice. Given the interneuron subtype diversity in L1,[37,38] we performed I_h recordings from interneurons with similar intrinsic electrophysiological properties, including the delay of the threshold spike, AP firing pattern, shape and amplitude of the after-hyperpolarization, and the amplitude of sag in response to hyperpolarizing currents. Voltage clamp experiments for I_h recordings in L1 interneurons were performed using the same voltage protocols as implemented for the hippocampal interneuron recordings. Similar to that in hippocampal interneurons, I_h was reduced in L1 interneurons from *Nf1*$^{+/-}$ mice (Supplementary Figure

6a). Moreover, and also consistent with our findings in hippocampal interneurons, the activation curve of I_h in L1 interneurons exhibited a hyperpolarizing shift of 8 mV in the half-activation potential in *Nf1*$^{+/-}$ mice (−88.8 ± 1.5 mV, $n = 13$) compared with their WT littermates (−81.0 ± 2.9 mV, $n = 8$, $P < 0.02$; Supplementary Figure 6b). Furthermore, and consistent with a significant downregulation of I_h, *Nf1*$^{+/-}$ L1 interneurons were more excitable than their WT controls (Supplementary Figure 6c). Taken together, our results establish that loss-of-function mutations in *Nf1* result in a decrease of I_h in GABAergic interneurons across multiple brain regions, which potentially represents a fundamental pathophysiological mechanism underlying NF1.

We next sought to determine whether a change in I_h, is sufficient to affect GABA release in *Nf1* mice. Hippocampal PV neurons primarily innervate postsynaptic neurons at the soma, providing strong inhibitory control over the firing properties of pyramidal neurons.[39] Therefore, alterations of the intrinsic excitability of PV neurons might affect action potential-driven synaptic GABA release onto pyramidal neurons. Accordingly, blocking I_h in WT mice would be expected to increase GABAergic input onto pyramidal neurons and mimic the enhanced inhibition observed in *Nf1*$^{9a-/9a-}$ mice. Indeed, consistent with our hypothesis, the frequency of spontaneous inhibitory postsynaptic currents (sIPSCs) recorded in CA1 pyramidal cells of WT mice was significantly increased after application of the HCN channel antagonist ZD7288 (30 μM; Supplementary Figures 7a and b). In contrast, no significant changes were observed in sIPSC amplitude (Supplementary Figure 7c). Taken together, these results support a causal influence of I_h in regulating inhibitory output from GABAergic interneurons onto CA1 pyramidal cells.

Constitutively active H-Ras/ERK signaling in *H-RAS*^{G12V} knock-in mice does not affect HCN current

NF1 is known to function as a negative regulator of Ras-ERK signaling. Therefore, to determine whether hyperactivation of the Ras-ERK pathway can affect HCN function, we made use of *H-Ras*^{G12V} knock-in mice, which express the constitutively active H-Ras^{G12V} isoform through a targeted mutation of the endogenous H-Ras gene.[40] H-Ras is the most prominent Ras isoform in the brain and is highly expressed in both interneurons and excitatory neurons.[25] *H-Ras*^{G12V} mice showed a dramatic increase of the Ras-ERK pathway, as measured by the relative level of phosphorylated ERK1 (212% of WT, $P < 0.01$) and ERK2 (246% of WT, $P < 0.001$) in the hippocampus, which is far greater than the levels of ERK activation observed in NF1 mice. However, in contrast to *Nf1* mutant mice, the current–voltage relationship and voltage dependence of I_h in PV neurons were similar between *H-Ras*^{G12V} and WT littermates (Supplementary Figures 8a–c; $V_{1/2}$: *H-Ras*^{G12V}, −84.7 ± 2.5 mV, $n = 6$; WT, −87.3 ± 1.7 mV, $n = 8$; $P = 0.3$). Furthermore, the slope of activation (*H-Ras*^{G12V}: 13.1 ± 1.2 mV mV, WT: 12.3 ± 0.7 mV; $P = 0.54$) and the I_h kinetics remained intact. Consistent with the absence of any detectable changes in I_h, neither the resting membrane potential (*H-Ras*^{G12V}: −62.5 ± 0.9 mV, $n = 8$ and WT: −63.9 ± 1.1 mV, $n = 12$; $P = 0.3$) nor the input resistance (*H-Ras*^{G12V}: 257 ± 29.2 MΩ, $n = 8$ and WT: 233 ± 27.5 MΩ, $n = 12$; $P = 0.57$) was altered in *H-Ras*^{G12V} PV neurons. Moreover, the excitability of PV neurons was also normal in *H-Ras*^{G12V} mice (Supplementary Figure 8d). These results show that marked activation of the Ras-ERK pathway is not sufficient to affect

I_h in PV neurons. Together with previous studies demonstrating that pharmacological inhibition of the ERK pathway has no effect on I_h in CA1 pyramidal neurons, as well as the absence of any consensus ERK phosphorylation sites on HCN1 or HCN2,[41] these results suggest that NF1 regulates HCN function through a H-Ras/ERK-independent mechanism.

The HCN channel agonist, LTG, rescues the electrophysiological and behavioral phenotypes of *Nf1* mice

LTG, a novel anticonvulsant which is known to act on Na^+ channels, has been also shown to enhance I_h in pyramidal neurons through a positive shift in the voltage dependence of I_h activation.[34] Therefore, we investigated whether LTG also enhances activation of I_h in GABAergic interneurons, and if so, whether it is able to restore the alterations in interneuron excitability in *Nf1* mice. I_h was recorded in $Nf1^{9a-/9a-}$ PV neurons in the presence of LTG (50 μM). Indeed, LTG increased the magnitude of I_h in $Nf1^{9a-/9a-}$ mice and caused a significant depolarizing shift in I_h activation in $Nf1^{9a-/9a-}$ PV neurons, which was fully normalized compared with recordings from WT mice (Figure 5a). The $V_{1/2}$ in the presence of LTG was −80.9 ± 2.0 mV (n = 9). LTG did not affect the slope of activation curve.

Next, we examined whether the LTG-mediated increase in I_h activation influences neuronal excitability. In the presence of LTG, the resting membrane potential of PV neurons was significantly depolarized in both $Nf1^{9a-/9a-}$ (3.5 ± 0.5 mV, n = 12) and WT mice (3.0 ± 0.3 mV, n = 9). Therefore, to examine the effect of LTG on action potential firing of PV neurons, the resting membrane potential was compensated to match the period preceding the application of LTG. Indeed, bath application of LTG caused a reduction of action potential firing rates in response to depolarizing current injections in $Nf1^{9a-/9a-}$ mice (Figure 5b). Furthermore, LTG application did not significantly affect action potential threshold, peak amplitude, half-width and rise time (Supplementary Table 4). To determine whether the effect of LTG on membrane excitability was directly mediated via I_h, the HCN antagonist ZD7288 was applied before application of LTG. In this condition, the effect of LTG on membrane excitability was fully blocked (Figure 5b). These results suggest that LTG decreases membrane excitability by directly increasing I_h activation, rather than by the blockade of Na^+ channels. Notably, this finding is entirely consistent with the notion that LTG exerts its anticonvulsant action on Na^+ channels selectively during periods of sustained depolarization or repetitive firing, as is the case during seizures.[42,43]

By decreasing interneuron excitability, LTG would be expected to significantly reduce inhibitory inputs onto neighboring pyramidal cells. Therefore, we examined the effect of LTG on LTP at Schaffer collateral-CA1 synapses. Indeed, LTG restored LTP in $Nf1^{9a-/9a-}$ mice to the level of WT mice, whereas the LTP deficit remained evident in vehicle-treated slices from $Nf1^{9a-/9a-}$ mice (Figure 5c). Together, our results with LTG provide increasing support for a causal model of NF1 pathophysiology by which the interneuron-specific reduction of I_h enhances GABAergic inhibition onto CA1 pyramidal neurons, leading to deficits in hippocampal LTP.

To further validate this model, we sought to determine whether the behavioral deficits of *Nf1* mice can also be rescued by LTG administration. Mice were given intraperitoneal injections of vehicle or LTG (25 mg kg^{-1}). There was a significant effect of training on the latency to

reach the platform, which was not modified by genotype or by treatment (Supplementary Figures 9a and b) and swimming speed was similar between different groups (Supplementary Figure 9c). As a replication of our previous results shown in Figure 1c, vehicle-treated $Nf1^{9a-/9a-}$ mice showed no spatial preference for the target quadrant. However, in strong support of our model of impaired HCN function in $Nf1^{9a-/9a-}$ mice, LTG treatment restored the learning capacity of $Nf1^{9a-/9a-}$ mice, without altering the performance of their WT littermates (Figure 5d). Furthermore, and consistent with a prominent influence of HCN channel function in the pathophysiology of the $Nf1^{+/-}$ mouse model, $Nf1^{+/-}$ mice treated with LTG also showed a clear preference for the target quadrant, in contrast to their vehicle-treated littermates (Figure 5e).

In addition to visual-spatial learning deficits, we recently demonstrated prominent impairments of motor coordination in NF1 patients, as well as in $Nf1^{+/-}$ mice.[5,44] In particular, $Nf1^{+/-}$ mice showed impaired learning on the accelerating rotarod, a motor learning paradigm that does not depend on hippocampal function. Indeed, LTG treatment completely rescued the motor coordination deficit in $Nf1^{+/-}$ mice (Supplementary Figure 9d). Taken together, using two different mouse models and highly distinct learning tasks, our results implicate the attenuation of HCN channel function as a novel therapeutic target for the treatment of cognitive and motor deficits in NF1.

DISCUSSION

Previous studies have shown that the learning and plasticity deficits of $Nf1^{+/-}$ mice result from enhanced neuronal inhibition,[3,6] suggesting that GABAergic interneurons are selectively impacted by NF1 loss-of-function mutations. Here, we developed a neuron-specific NF1 exon 9a mutant ($Nf1^{9a-/9a-}$), in order to more specifically explore the neuronal pathophysiology underlying NF1. $Nf1^{9a-/9a-}$ mice showed the same pathophysiological phenotype as the $Nf1^{+/-}$ mice. By using proteomics and electrophysiological techniques, we identified a cell-type-specific attenuation of I_h in GABAergic interneurons, which strongly contributes to the observed enhanced inhibition in *Nf1* loss-of-function mice. Importantly, we found that stimulating HCN current with the clinically approved drug LTG rescues the deficits in synaptic plasticity, motor performance and spatial learning in both $Nf1^{9a-/9a-}$ and $Nf1^{+/-}$ mice.

Our findings suggest that I_h could be an important modulator of synaptic plasticity and spatial memory by regulating inhibitory outputs. Consistent with this notion, blocking HCN channels resulted in increased frequency of sIPSCs in pyramidal neurons. As the majority of spontaneous inhibitory events onto hippocampal pyramidal neurons arise from perisomatic inhibition,[45,46] it is likely that the increased frequency of sIPSCs is predominantly mediated by PV neurons. However, the contribution of other interneurons subtypes, including dendritically targeting interneurons such as OA interneurons, cannot be excluded.

Notably, in both *Nf1* mutants, we observed a downregulation of I_h associated with increased excitability of GABAergic interneurons. In particular, we observed a decrease of I_h and corresponding increase of intrinsic excitability in all three types of interneurons tested in this study: hippocampal PV interneurons, hippocampal OA interneurons and L1 visual cortex

interneurons. This suggests that the interneuron-specific impairment of HCN function is evident in a wide diversity of interneuron subtypes across multiple brain regions. Our finding that a reduction in I_h was consistently associated with an increase of intrinsic excitability is also consistent with previous reports in pyramidal neurons where downregulation of I_h increased EPSP amplitude, temporal summation and intrinsic excitability.[16,20,47] The regulatory effect of I_h on membrane excitability has been attributed to its partial activity at resting membrane potentials, resulting in a shunt conductance, which decreases the temporal integration of EPSPs.[16,34] In addition, HCN channels have been shown to provide a tonic depolarizing current that increases resting activation of the delayed-rectifier M-type K^+ channels along with inactivation of N- and T-type voltage-gated Ca^{2+} channels.[48,49]

Currently, there are no specific agonists for HCN channels. Therefore, we used the commonly prescribed anticonvulsant LTG, which is well established to enhance I_h and decrease excitability in pyramidal neurons.[34] Although LTG is also known to inhibit Na^+ channels, it acts mainly on the slow inactivated state with no effect on the resting, closed state.[42,43] This suggests that LTG, at clinically relevant concentrations, exerts its anticonvulsant action on Na^+ channels upon prolonged depolarization or repetitive firing conditions, as is the case during seizures. Accordingly, we observed no significant changes in LTP or learning with LTG treatment in WT mice. Furthermore, the LTG-induced decrease in membrane excitability was not associated with a change in action potential parameters and it was blocked by prior application of the highly specific HCN antagonist ZD7288, suggesting that LTG conferred its action mainly through I_h rather than through changes in sodium channel conductance.

Although inhibition of Ras/ERK signaling has previously been shown to be sufficient to reverse the increased inhibition and cognitive deficits in *Nf1* mutant mice,[3,6,29] the particularly large size and multi-domain structure of NF1 have led many investigators to hypothesize that NF1 might have functions beyond its well-established role as a negative regulator of Ras signaling. Here, we have shown that NF1 interacts with HCN1 through its N-terminus, and that mutations in NF1 affect HCN channel function. The regulation of HCN channels could be Ras independent, as HCN channels lack ERK consensus phosphorylation sites and I_h is not affected by MEK inhibitors.[41] Moreover, using *H-Ras*^{G12V} knock-in mice (a mouse model for Costello syndrome), we show that a marked increase of Ras-ERK signaling is insufficient to change I_h in interneurons. Recently, a mouse model of Noonan syndrome has been described, which demonstrated that upregulation of the ERK signaling pathway causes learning and LTP deficits, which are at least in part mediated by increased glutamatergic synaptic transmission.[50] Hence, the interneuron-specific phenotype of NF1 does not seem to be common phenotype of the Rasopathy family, which could indicate a distinct, Ras-independent function of the NF1 protein. A Ras-independent function of neuronal NF1 has been previously identified in the *Drosophila* model of NF1, and in neuronal cultures from *Nf1* mice, through alterations in cyclic adenosine monophosphate (cAMP) signaling.[51–53] Given that HCN channels are well-known to be regulated by cAMP,[13] it is distinctly possible that the HCN1–NF1 interaction affects local changes in cAMP, which contribute to the attenuated I_h current in interneurons of *Nf1* mice.[54] Further studies are needed to address these possibilities. From a therapeutic perspective, it is notable

that normalization of both Ras/ERK signaling and HCN function appear sufficient to rescue the electrophysiological and learning deficits in mice. However, as targeted downregulation of Ras/ERK signaling have shown no evidence of clinical efficacy in children with NF1,[8,9] targeting the HCN-dependent increase in the excitability of inhibitory neurons might have important therapeutic implications for the treatment of NF1 patients, either as monotherapy or in combination with Ras/ERK inhibitors.

Taken together, using two different *Nf1* loss-of-function mutants, we have elucidated a novel cell-type-specific pathophysiological mechanism underlying NF1, by which interneuron excitability, synaptic plasticity, cognitive function and motor coordination can all be rescued by the clinically approved HCN agonist LTG. Therefore, HCN channels are a highly promising drug target for treating the cognitive deficits associated with NF1.

Supplementary Material

Refer to Web version on PubMed Central for supplementary material.

Acknowledgments

We thank Dr Nolan for providing the HCN-KO brain samples, Dr Chetkovich for the guinea pig HCN1 antibody, Dr Siegelbaum for the HCN1 constructs, Dr Guerra and Dr Barbacid for the *H-Ras*^{G12V} mice, and TEVA Pharmaceuticals for providing LTG. We are grateful to the following people for their assistance: M Aghadavoud Jolfaei (field-recording and genotyping), E Haasdijk and E Goedknegt (immunohistochemistry), M Elgersma, U Unmehopa and D Swaab (*in-situ* hybridizations), RC van der Schors (mass spectrometry), Kelly Diggs-Andrews (NF1 western blot) and R Bari (cloning *Nf1* 9a gene). We thank Gerard Borst for advice and critical reading of the manuscript. This work was supported by a Children Tumor Foundation (CTF) young investigator award to AO, by grants from the Netherlands Brain Foundation (HsN) and NWO-ZonMW (VICI) to YE, a Department of Defense grant to DHG, HEALTH-2009-2.1.2-1 EU-FP7 SYNSYS to ABS and KWL, and a FES-NEUROBASIC grant to CNL, ABS, SAK and YE.

References

1. Krab LC, Aarsen FK, de Goede-Bolder A, Catsman-Berrevoets CE, Arts WF, Moll HA, et al. Impact of neurofibromatosis type 1 on school performance. J Child Neurol. 2008; 23:1002–1010. [PubMed: 18827266]
2. Hyman SL, Shores A, North KN. The nature and frequency of cognitive deficits in children with neurofibromatosis type 1. Neurology. 2005; 65:1037–1044. [PubMed: 16217056]
3. Costa RM, Federov NB, Kogan JH, Murphy GG, Stern J, Ohno M, et al. Mechanism for the learning deficits in a mouse model of neurofibromatosis type 1. Nature. 2002; 415:526–530. [PubMed: 11793011]
4. Silva AJ, Frankland PW, Marowitz Z, Friedman E, Laszlo GS, Cioffi D, et al. A mouse model for the learning and memory deficits associated with neurofibromatosis type I. Nat Genet. 1997; 15:281–284. [PubMed: 9054942]
5. van der Vaart T, van Woerden GM, Elgersma Y, de Zeeuw CI, Schonewille M. Motor deficits in neurofibromatosis type 1 mice: the role of the cerebellum. Genes Brain Behav. 2011; 10:404–409. [PubMed: 21352477]
6. Cui Y, Costa RM, Murphy GG, Elgersma Y, Zhu Y, Gutmann DH, et al. Neurofibromin regulation of ERK signaling modulates GABA release and learning. Cell. 2008; 135:549–560. [PubMed: 18984165]
7. Ye X, Carew TJ. Small G protein signaling in neuronal plasticity and memory formation: the specific role of ras family proteins. Neuron. 2010; 68:340–361. [PubMed: 21040840]

8. Krab LC, de Goede-Bolder A, Aarsen FK, Pluijm SM, Bouman MJ, van der Geest JN, et al. Effect of simvastatin on cognitive functioning in children with neurofibromatosis type 1: a randomized controlled trial. JAMA. 2008; 300:287–294. [PubMed: 18632543]
9. van der Vaart T, Plasschaert E, Rietman AB, Renard M, Oostenbrink R, Vogels A, et al. Simvastatin for cognitive deficits and behavioural problems in patients with neurofibromatosis type 1 (NF1-SIMCODA): a randomised, placebo-controlled trial. Lancet Neurol. 2013; 12:1076–1083. [PubMed: 24090588]
10. Geist RT, Gutmann DH. Expression of a developmentally-regulated neuron-specific isoform of the neurofibromatosis 1 (NF1) gene. Neurosci Lett. 1996; 211:85–88. [PubMed: 8830850]
11. Gutmann DH, Zhang Y, Hirbe A. Developmental regulation of a neuron-specific neurofibromatosis 1 isoform. Ann Neurol. 1999; 46:777–782. [PubMed: 10553997]
12. Danglot G, Regnier V, Fauvet D, Vassal G, Kujas M, Bernheim A. Neurofibromatosis 1 (NF1) mRNAs expressed in the central nervous system are differentially spliced in the 5' part of the gene. Hum Mole Genet. 1995; 4:915–920.
13. Wahl-Schott C, Biel M. HCN channels: structure, cellular regulation and physiological function. Cell Mol Life Sci. 2009; 66:470–494. [PubMed: 18953682]
14. Maccaferri G, McBain CJ. The hyperpolarization-activated current (Ih) and its contribution to pacemaker activity in rat CA1 hippocampal stratum oriens-alveus interneurones. J Physiol. 1996; 497:119–130. [PubMed: 8951716]
15. Lupica CR, Bell JA, Hoffman AF, Watson PL. Contribution of the hyperpolarization-activated current (I(h)) to membrane potential and GABA release in hippocampal interneurons. J Neurophysiol. 2001; 86:261–268. [PubMed: 11431507]
16. Magee JC. Dendritic Ih normalizes temporal summation in hippocampal CA1 neurons. Nat Neurosci. 1999; 2:848.
17. Nolan MF, Malleret G, Dudman JT, Buhl DL, Santoro B, Gibbs E, et al. A behavioral role for dendritic integration: HCN1 channels constrain spatial memory and plasticity at inputs to distal dendrites of CA1 pyramidal neurons. Cell. 2004; 119:719–732. [PubMed: 15550252]
18. Wang M, Ramos BP, Paspalas CD, Shu Y, Simen A, Duque A, et al. Alpha2A-adrenoceptors strengthen working memory networks by inhibiting cAMP-HCN channel signaling in prefrontal cortex. Cell. 2007; 129:397–410. [PubMed: 17448997]
19. Brager DH, Akhavan AR, Johnston D. Impaired dendritic expression and fmr1(-) (/y) plasticity of h-channels in the mouse model of fragile × syndrome. Cell Rep. 2012; 1:225–233. [PubMed: 22662315]
20. Shah MM, Anderson AE, Leung V, Lin X, Johnston D. Seizure-induced plasticity of h channels in entorhinal cortical layer III pyramidal neurons. Neuron. 2004; 44:495–508. [PubMed: 15504329]
21. Fan Y, Fricker D, Brager DH, Chen X, Lu HC, Chitwood RA, et al. Activity-dependent decrease of excitability in rat hippocampal neurons through increases in I(h). Nat Neurosci. 2005; 8:1542–1551. [PubMed: 16234810]
22. Notomi T, Shigemoto R. Immunohistochemical localization of Ih channel subunits, HCN1–4, in the rat brain. J Comp Neurol. 2004; 471:241–276. [PubMed: 14991560]
23. Bender RA, Brewster A, Santoro B, Ludwig A, Hofmann F, Biel M, et al. Differential and age-dependent expression of hyperpolarization-activated, cyclic nucleotide-gated cation channel isoforms 1–4 suggests evolving roles in the developing rat hippocampus. Neuroscience. 2001; 106:689–698. [PubMed: 11682156]
24. Brewster AL, Chen Y, Bender RA, Yeh A, Shigemoto R, Baram TZ. Quantitative analysis and subcellular distribution of mRNA and protein expression of the hyperpolarization-activated cyclic nucleotide-gated channels throughout development in rat hippocampus. Cereb Cortex. 2007; 17:702–712. [PubMed: 16648453]
25. Sugino K, Hempel CM, Miller MN, Hattox AM, Shapiro P, Wu C, et al. Molecular taxonomy of major neuronal classes in the adult mouse forebrain. Nat Neurosci. 2006; 9:99–107. [PubMed: 16369481]
26. Zeng H, Shen EH, Hohmann JG, Oh SW, Bernard A, Royall JJ, et al. Large-scale cellular-resolution gene profiling in human neocortex reveals species-specific molecular signatures. Cell. 2012; 149:483–496. [PubMed: 22500809]

27. van Woerden GM, Harris KD, Hojjati MR, Gustin RM, Qiu S, de Avila Freire R, et al. Rescue of neurological deficits in a mouse model for Angelman syndrome by reduction of alphaCaMKII inhibitory phosphorylation. Nat Neurosci. 2007; 10:280–282. [PubMed: 17259980]
28. Ozonoff S. Cognitive impairment in neurofibromatosis type 1. Am J Med Genet. 1999; 89:45–52. [PubMed: 10469436]
29. Li W, Cui Y, Kushner SA, Brown RA, Jentsch JD, Frankland PW, et al. The HMG-CoA reductase inhibitor lovastatin reverses the learning and attention deficits in a mouse model of neurofibromatosis type 1. Curr Biol. 2005; 15:1961–1967. [PubMed: 16271875]
30. Larson J, Wong D, Lynch G. Patterned stimulation at the theta frequency is optimal for the induction of hippocampal long-term potentiation. Brain Res. 1986; 368:347–350. [PubMed: 3697730]
31. Chapman CA, Perez Y, Lacaille JC. Effects of GABA(A) inhibition on the expression of long-term potentiation in CA1 pyramidal cells are dependent on tetanization parameters. Hippocampus. 1998; 8:289–298. [PubMed: 9662142]
32. Bollag G, McCormick F, Clark R. Characterization of full-length neurofibromin: tubulin inhibits Ras GAP activity. EMBO J. 1993; 12:1923–1927. [PubMed: 8491185]
33. Gregory PE, Gutmann DH, Mitchell A, Park S, Boguski M, Jacks T, et al. Neurofibromatosis type 1 gene product (neurofibromin) associates with microtubules. Somat Cell Mol Genet. 1993; 19:265–274. [PubMed: 8332934]
34. Poolos NP, Migliore M, Johnston D. Pharmacological upregulation of h-channels reduces the excitability of pyramidal neuron dendrites. Nat Neurosci. 2002; 5:767–774. [PubMed: 12118259]
35. Molosh AI, Johnson PL, Spence JP, Arendt D, Federici LM, Bernabe C, et al. Social learning and amygdala disruptions in Nf1 mice are rescued by blocking p21-activated kinase. Nat Neurosci. 2014; 17:1583–1590. [PubMed: 25242307]
36. Shilyansky C, Karlsgodt KH, Cummings DM, Sidiropoulou K, Hardt M, James AS, et al. Neurofibromin regulates corticostriatal inhibitory networks during working memory performance. Proc Natl Acad Sci USA. 2010; 107:13141–13146. [PubMed: 20624961]
37. Lee S, Hjerling-Leffler J, Zagha E, Fishell G, Rudy B. The largest group of superficial neocortical GABAergic interneurons expresses ionotropic serotonin receptors. J Neurosci. 2010; 30:16796–16808. [PubMed: 21159951]
38. Rudy B, Fishell G, Lee S, Hjerling-Leffler J. Three groups of interneurons account for nearly 100% of neocortical GABAergic neurons. Deve Neurobiol. 2011; 71:45–61.
39. Pawelzik H, Hughes DI, Thomson AM. Physiological and morphological diversity of immunocytochemically defined parvalbumin- and cholecystokinin-positive interneurones in CA1 of the adult rat hippocampus. J Comp Neurol. 2002; 443:346–367. [PubMed: 11807843]
40. Schuhmacher AJ, Guerra C, Sauzeau V, Canamero M, Bustelo XR, Barbacid M. A mouse model for Costello syndrome reveals an Ang II-mediated hypertensive condition. J Clin Invest. 2008; 118:2169–2179. [PubMed: 18483625]
41. Poolos NP, Bullis JB, Roth MK. Modulation of h-channels in hippocampal pyramidal neurons by p38 mitogen-activated protein kinase. J Neurosci. 2006; 26:7995–8003. [PubMed: 16870744]
42. Kuo CC, Lu L. Characterization of lamotrigine inhibition of Na+ channels in rat hippocampal neurones. Br J Pharmacol. 1997; 121:1231–1238. [PubMed: 9249262]
43. Xie X, Lancaster B, Peakman T, Garthwaite J. Interaction of the antiepileptic drug lamotrigine with recombinant rat brain type IIA Na+ channels and with native Na + channels in rat hippocampal neurones. Pflugers Archiv: Eur J Physiol. 1995; 430:437–446. [PubMed: 7491269]
44. Krab LC, de Goede-Bolder A, Aarsen FK, Moll HA, De Zeeuw CI, Elgersma Y, et al. Motor learning in children with neurofibromatosis type I. Cerebellum. 2011; 10:14–21. [PubMed: 20927664]
45. Miles R, Toth K, Gulyas AI, Hajos N, Freund TF. Differences between somatic and dendritic inhibition in the hippocampus. Neuron. 1996; 16:815–823. [PubMed: 8607999]
46. Soltesz I, Smetters DK, Mody I. Tonic inhibition originates from synapses close to the soma. Neuron. 1995; 14:1273–1283. [PubMed: 7605636]

47. Brager DH, Johnston D. Plasticity of intrinsic excitability during long-term depression is mediated through mGluR-dependent changes in I(h) in hippocampal CA1 pyramidal neurons. J Neurosci. 2007; 27:13926–13937. [PubMed: 18094230]

48. George MS, Abbott LF, Siegelbaum SA. HCN hyperpolarization-activated cation channels inhibit EPSPs by interactions with M-type K(+) channels. Nat Neurosci. 2009; 12:577–584. [PubMed: 19363490]

49. Tsay D, Dudman JT, Siegelbaum SA. HCN1 channels constrain synaptically evoked Ca2+ spikes in distal dendrites of CA1 pyramidal neurons. Neuron. 2007; 56:1076–1089. [PubMed: 18093528]

50. Lee YS, Ehninger D, Zhou M, Oh JY, Kang M, Kwak C, et al. Mechanism and treatment for learning and memory deficits in mouse models of Noonan syndrome. Nat Neurosci. 2014; 17:1736–1743. [PubMed: 25383899]

51. Brown JA, Gianino SM, Gutmann DH. Defective cAMP generation underlies the sensitivity of CNS neurons to neurofibromatosis-1 heterozygosity. J Neurosci. 2010; 30:5579–5589. [PubMed: 20410111]

52. The I, Hannigan GE, Cowley GS, Reginald S, Zhong Y, Gusella JF, et al. Rescue of a Drosophila NF1 mutant phenotype by protein kinase A. Science. 1997; 276:791–794. [PubMed: 9115203]

53. Tong J, Hannan F, Zhu Y, Bernards A, Zhong Y. Neurofibromin regulates G protein-stimulated adenylyl cyclase activity. Nat Neurosci. 2002; 5:95–96. [PubMed: 11788835]

54. Stowe IB, Mercado EL, Stowe TR, Bell EL, Oses-Prieto JA, Hernandez H, et al. A shared molecular mechanism underlies the human rasopathies Legius syndrome and Neurofibromatosis-1. Genes Dev. 2012; 26:1421–1426. [PubMed: 22751498]

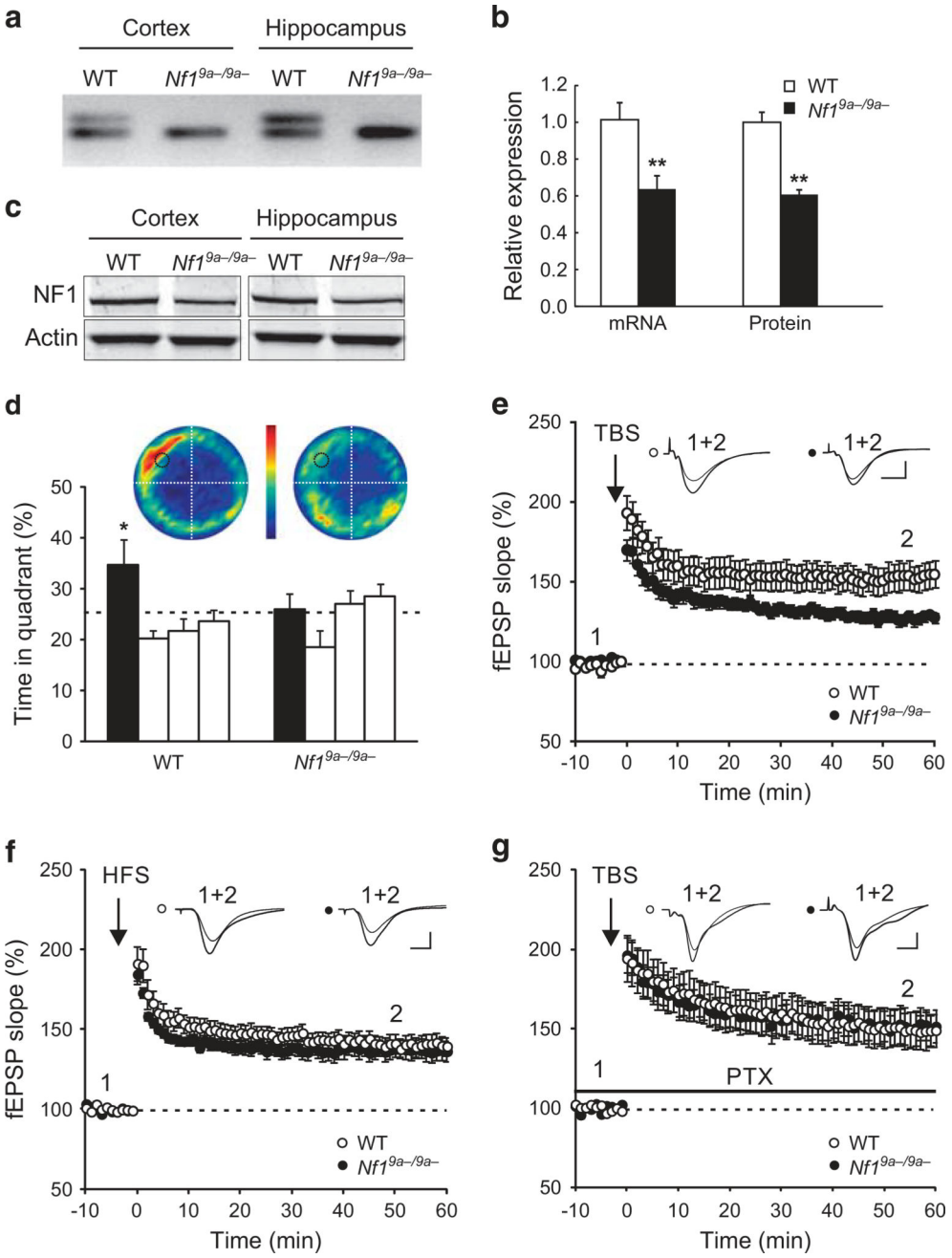

Figure 1.

Characterization of the *Nf1*$^{9a-/9a-}$ mutant. (**a**) Results of the reverse transcription-PCR in cortex and hippocampus in WT and *Nf1*$^{9a-/9a-}$ mice showing loss of Nf1 exon 9a-containing transcripts in *Nf1*$^{9a-/9a-}$ mice (representative image, quantitative PCR experiment performed on 7 WT and 9 mutant mice). (**b**) Western blots of cortical and hippocampal lysates of the WT and *Nf1*$^{9a-/9a-}$ mice showing reduction of total neurofibromin levels in the mutants (representative image, experiment performed on 10 WT and 11 mutant mice). (**c**) *Nf1* mRNA (*Nf1*$^{9a-/9a-}$: $n = 9$; WT: $n = 7$, $P < 0.01$) and neurofibromin protein (*Nf1*$^{9a-/9a-}$: $n = 11$; WT: $n = 10$, $P < 0.001$) in the hippocampus of WT and *Nf1*$^{9a-/9a-}$ mice. (**d**) In the water

maze probe trial, $Nf1^{9a-/9a-}$ mice show no significant spatial learning, while WT mice show a clear preference for the target quadrant (TQ, black column) ($Nf1^{9a-/9a-}$: $n = 15$, $P = 0.6$; WT: $n = 14$, $P < 0.001$, paired t-test between target and average of other quadrants). Bars represent target, adjacent right, opposite, and adjacent left quadrants, respectively. The heat-plots are a visual representation of all search tracks, in which the color indicates the mean time spent at a certain position. The black circle indicates the target platform position used during training. (**e**) LTP deficit at Schaffer collateral-CA1 synapses in $Nf1^{9a-/9a-}$ mice induced by TBS (WT: $n = 14$ and $Nf1^{9a-/9a-}$: $n = 15$; $P < 0.02$) but not by an (**f**) High frequency stimulation (WT: $n = 13$ and $Nf1^{9a-/9a-}$: $n = 15$, $P = 0.8$). (**g**) Picrotoxin (PTX) restores TBS-LTP in $Nf1^{9a-/9a-}$ mice (WT: $n = 14$ and $Nf1^{9a-/9a-}$: $n = 17$, $P = 0.9$). Insets are field excitatory postsynaptic potentials (fEPSPs) in WT and $Nf1^{9a-/9a-}$ mice taken at the points shown in each graph. Calibration: 5 ms and 0.2 mV. Statistical analyses were performed by Student's *t*-test. $^{*}P < 0.05$, $^{**}P < 0.01$. Data represent the mean ± s.e.m.

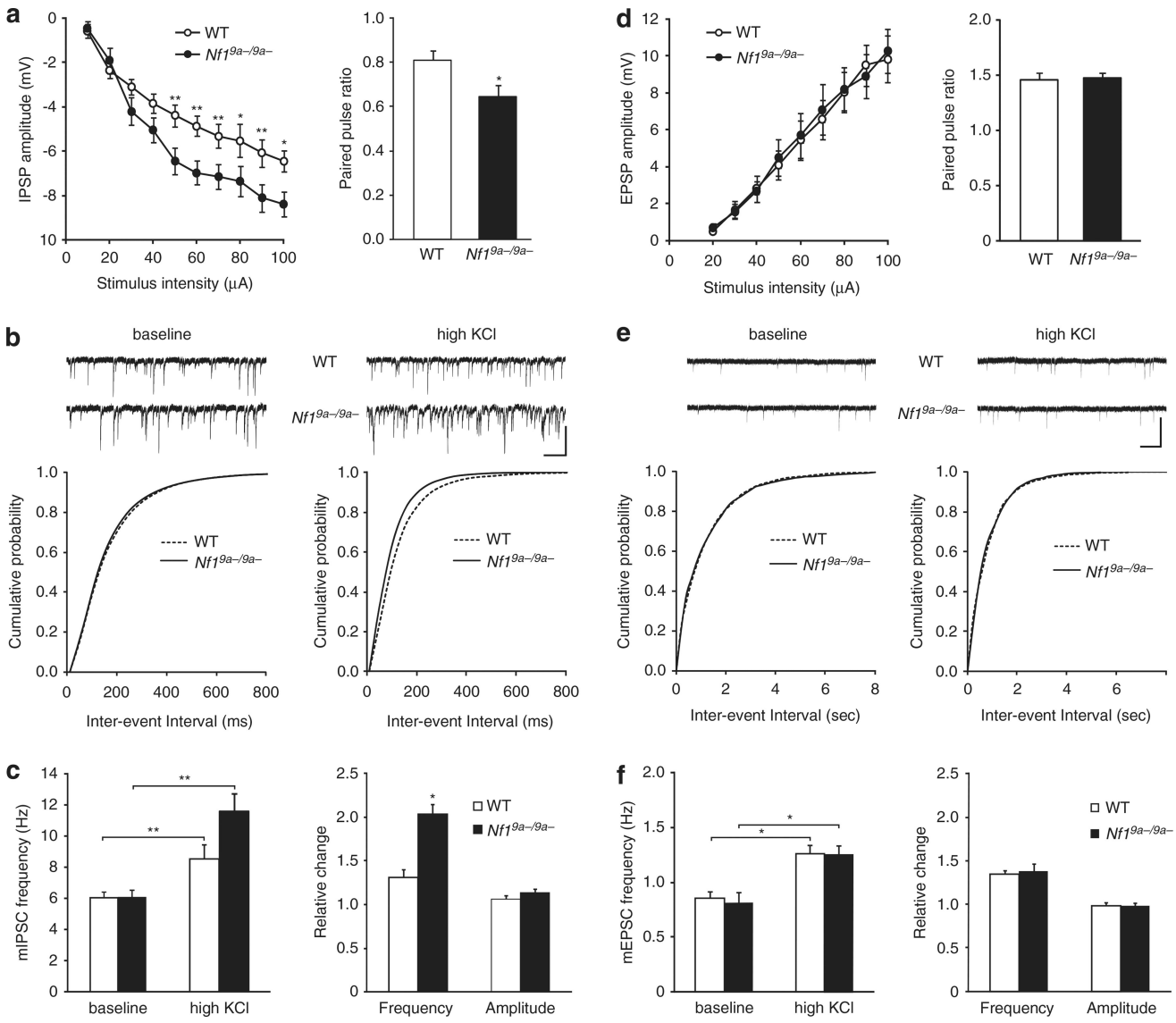

Figure 2.

Enhanced inhibition in *Nf1*$^{9a-/9a-}$ mice. (**a**) Evoked inhibitory postsynaptic potentials (IPSPs) show larger amplitude in mutants (two-way analysis of variance (ANOVA), $F_{1,16}$ = 5.3; $P < 0.05$; $n = 9$ for both groups) and paired-pulse ratio is reduced in *Nf1*$^{9a-/9a-}$ compared with WT controls (0.6 ± 0.04, $n = 10$ vs 0.8 ± 0.05, $n = 7$; $P < 0.02$). (**b**) Representative traces (top) and cumulative distributions of miniature inhibitory postsynaptic current (mIPSC) inter-event intervals (bottom) showing a significant leftward shift of the curve in *Nf1*$^{9a-/9a-}$ pyramidal neurons under high KCl (Kolmogorov–Smirnov test, P < 0.001), but not with normal KCl (Kolmogorov–Smirnov test, $P = 0.3$). (**c**) Group data of mIPSC frequency in baseline and high KCl conditions. High KCl results in a significant increase in mIPSC frequency for both WT (6 ± 0.5 Hz vs 9 ± 0.9 Hz, $n = 12$; $P < 0.004$) and *Nf1*$^{9a-/9a-}$ mice (6 ± 0.5 Hz vs 12 ± 1.0 Hz, $n = 11$; $P < 0.0005$). Overall, the ratio of mean frequency of the events in high KCl to that in baseline condition is higher in mutants ($P <$ 0.001), whereas the mean amplitude remains unchanged. (**d**) Evoked excitatory postsynaptic

potentials (EPSPs) show no difference in amplitude (two-way ANOVA, $F_{1,17} = 0.03$; $P = 0.9$, WT: $n = 9$, $Nf1^{9a-/9a-}$: $n = 10$) or paired-pulse ratio ($Nf1^{9a-/9a-}$: 1.5 ± 0.5, $n = 10$; WT: 1.5 ± 0.1, $n = 9$; $P = 0.8$). (**e**) Representative traces (top) and cumulative distributions of miniature excitatory postsynaptic current (mEPSC) inter-event intervals (bottom) for which there is no significant difference in the cumulative distribution during baseline or high KCl conditions ($P = 0.35$). (**f**) Group data of mEPSC frequency in baseline and high KCl conditions (WT: 0.9 ± 0.1 Hz vs 1.26 ± 0.1 Hz, $n = 9$, $P < 0.05$; $Nf1^{9a-/9a-}$: 0.8 ± 0.1 Hz, vs 1.25 ± 0.1 Hz, $n = 10$, $P < 0.05$). The ratio of mean frequency of mEPSC in high KCl to that in baseline conditions is unchanged ($P = 0.9$). Calibration: 500 ms and 100 pA. *$P < 0.05$, **$P < 0.01$. Data represent the mean ± s.e.m.

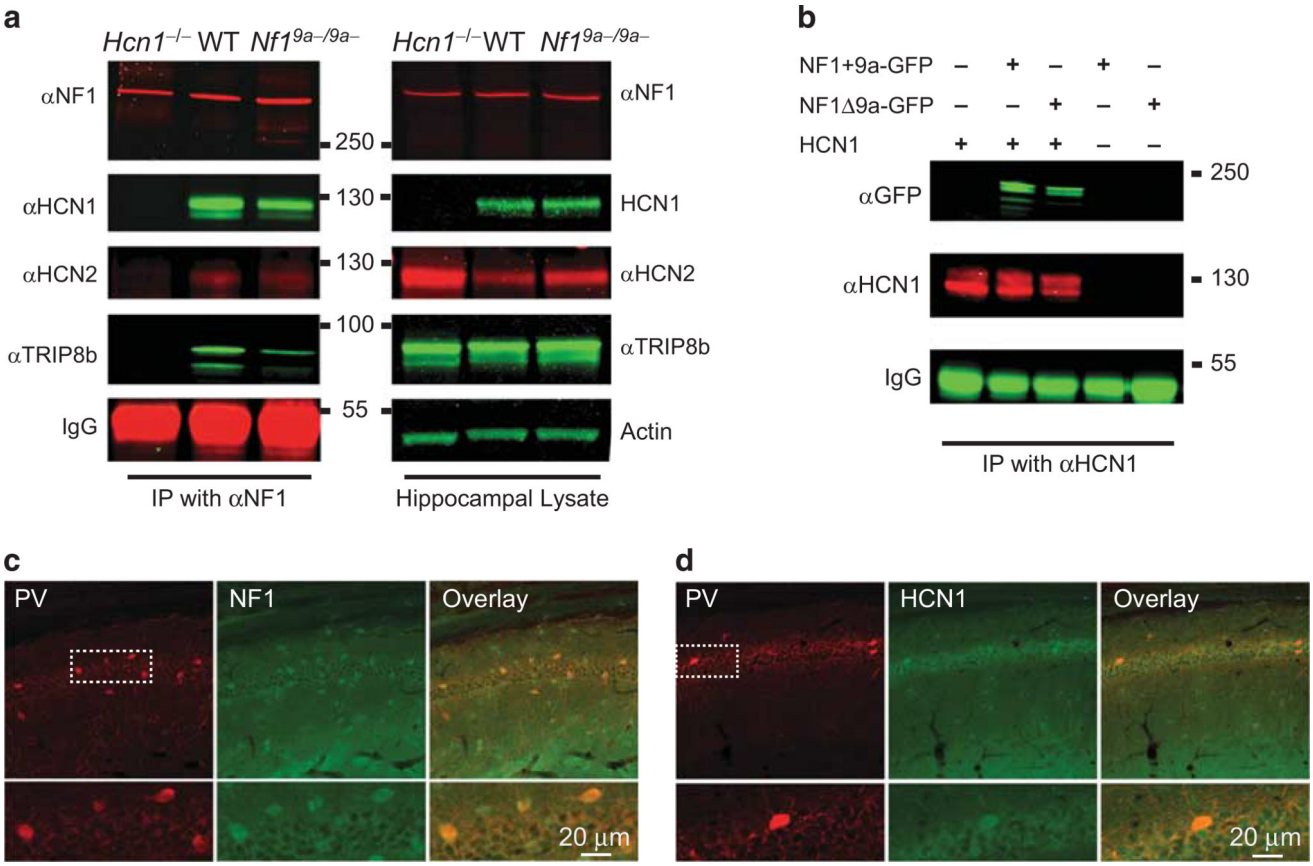

Figure 3.

Hyperpolarization-activated cyclic nucleotide-gated 1 (HCN1) is identified as an Neurofibromatosis type 1 (NF1)-interacting protein and enriched in parvalbumin (PV) neurons. (**a**) Immunoprecipitation (IP) using an antibody directed against neurofibromin on hippocampal lysates from WT, *Hcn1*$^{-/-}$ and *Nf1*$^{9a-/9a-}$ mice (representative image; IP on WT and *Nf1*$^{9a-/9a-}$ lysates has been successfully repeated four times, and two times on *Hcn1*$^{-/-}$ lysates. Immunoblotting analysis was performed using the antibodies as indicated (left panel). HCN1, HCN2 and TRIP8b were all co-precipitated with NF1 in the WT and *Nf1*$^{9a-/9a-}$ samples. In the absence of HCN1 (*Hcn1*$^{-/-}$), the NF1 antibody is unable to co-immunoprecipitation (co-IP) HCN2 and TRIP8b. Right panel: hippocampal lysates used as input for IP experiments, showing normal HCN1, HCN2 and TRIP8b expression in *Nf1*$^{9a-/9a-}$ mice. (**b**) Co-IP using a monoclonal antibody against HCN1 on lysates made from HEK293T cells co-transfected with constructs expressing HCN1 and the N-terminal half of NF1 (with or without exon 9a) fused to GFP (representative image; transfection and IP were repeated two times). Immunoblot analysis was performed with antibodies directed against HCN1 and GFP. (**c** and **d**) Immunofluorescence co-labeling of PV (red) and NF1 (green) (**c**), or PV (red) and HCN1 (green) (**d**) in hippocampal sections of WT mice, showing high expression of NF1 and HCN1 in PV-expressing neurons.

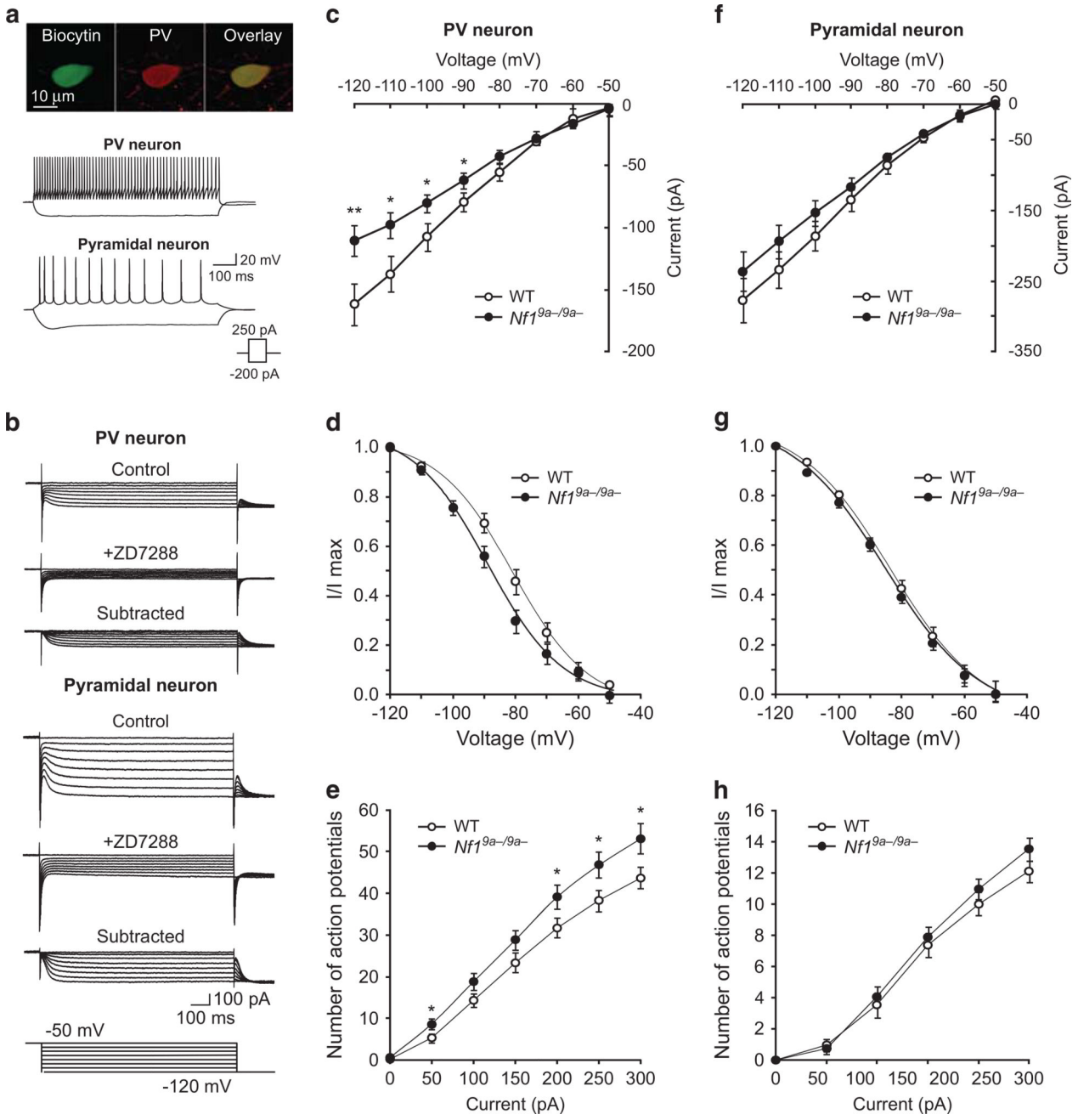

Figure 4.

I_h is selectively attenuated in *Nf1*$^{9a-/9a-}$ PV neurons. (**a**) Top: PV immunoreactivity of a biocytin-filled interneuron shown by fluorescent double labeling (representative image, repeated for each included interneuron). Bottom: Representative voltage responses of PV and pyramidal neurons to depolarizing and hyperpolarizing current injections. (**b**) Sample voltage–clamp recordings from a PV neuron and a pyramidal neuron. The ZD7288-sensitive I_h currents were obtained by subtracting current traces before and after application of (30 µM) ZD7288. Currents were evoked by 800 ms hyperpolarizing voltage steps from a holding potential of −50 to −120 mV in 10 mV increments. (**c**) The current–voltage (*I–V*)

relationship of I_h is significantly shifted toward smaller I_h in $Nf1^{9a-/9a-}$ PV neurons ($F_{1,16}$ = 4.1, $P < 0.05$, $n = 7$ and $n = 11$ for WT and $Nf1^{9a-/9a-}$, respectively). (**d**) The activation curve of I_h obtained by plotting the normalized tail current amplitude as a function of the voltage step and fitted with a Boltzmann function (solid lines). There was a significant hyperpolarizing shift in the voltage-dependent activation of I_h in $Nf1^{9a-/9a-}$ PV neurons ($V_{1/2}$ in WT was −81.2 ± 2.0 and −88.4 ± 1.9 in $Nf1^{9a-/9a-}$, $P < 0.01$). (**e**) The mean number of action potentials generated in response to depolarizing current pulses in the PV neurons from $Nf1^{9a-/9a-}$ is significantly higher ($F_{1,22}$ = 4.4, $P < 0.05$). (**f**) No significant differences were found in the *I–V* relationship ($F_{1,19}$ = 1.4, $P = 0.2$) or in (**g**) the voltage dependence of I_h activation of pyramidal neurons between genotypes ($P = 0.3$; $n = 9$ and $n = 10$ for WT and $Nf1^{9a-/9a-}$, respectively). (**h**) Excitability of pyramidal neurons is unchanged in $Nf1^{9a-/9a-}$ mice ($F_{1,32}$ = 0.1, $P = 0.8$; $n = 16$ and $n = 18$ for WT and $Nf1^{9a-/9a-}$, respectively). Statistical analyses were performed by Student's *t*-test and two-way ANOVA followed by Tukey's test. $^*P < 0.05$, $^{**}P < 0.01$. Data represent the mean ± s.e.m.

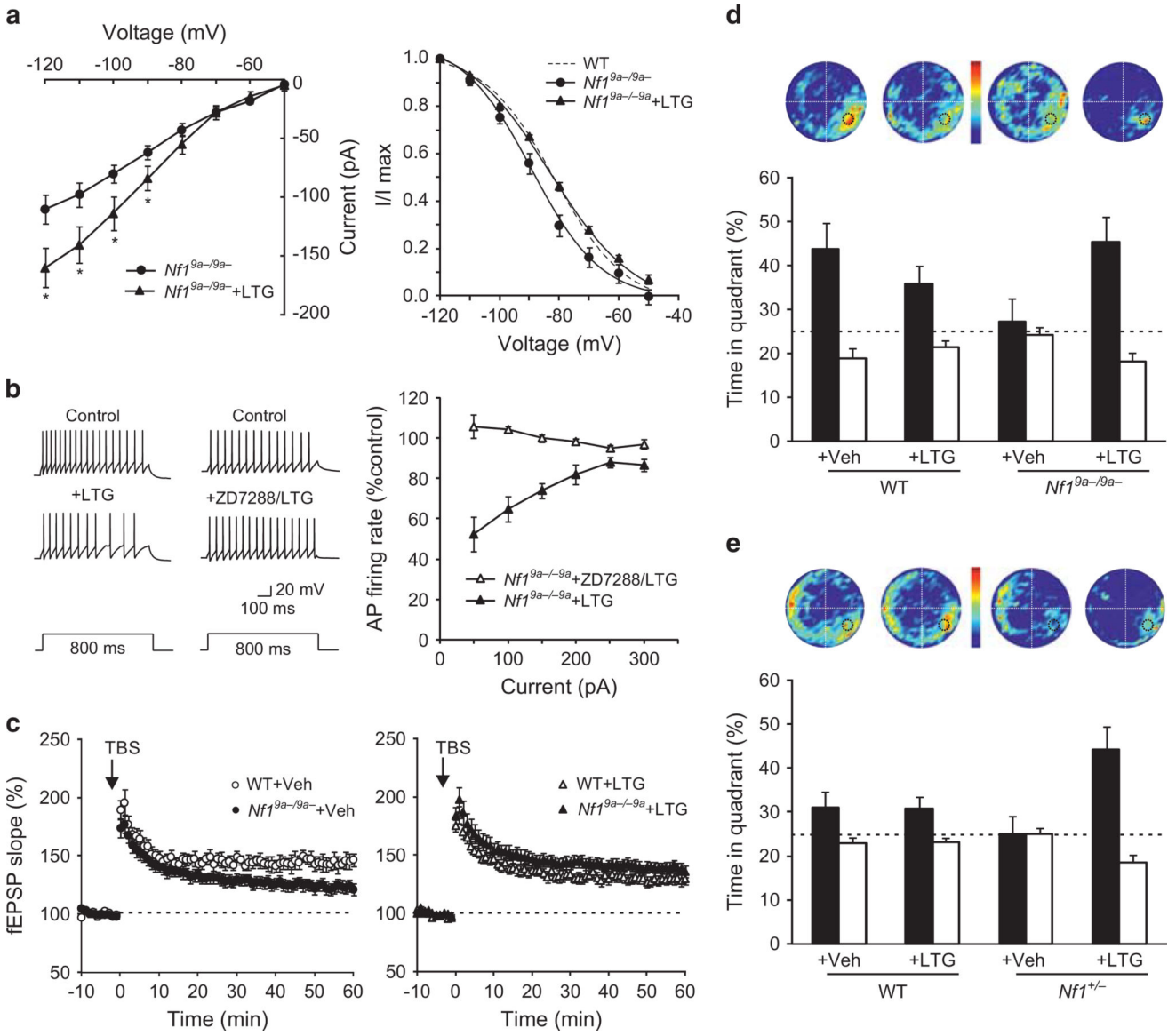

Figure 5.

Lamotrigine (LTG) rescues the electrophysiological and behavioral phenotypes in *Nf1*$^{9a-/9a-}$ mice. (**a**) Left: I_h amplitude is significantly increased by LTG in *Nf1*$^{9a-/9a-}$ mice ($F_{1,21}$ = 9.9, $P < 0.05$, $n = 12$). Right: LTG shifts I_h activation to more depolarized potentials in PV neurons from *Nf1*$^{9a-/9a-}$ mice. Control data are the same as shown in Figures 4c and d. Dashed line shows activation curve for wild-type (WT) littermates. (**b**) LTG decreases membrane excitability in PV neurons from *Nf1*$^{9a-/9a-}$ mice and this effect is blocked by ZD7288. Left: sample recordings of APs elicited by a depolarizing current step before and after application of LTG in the absence and presence of ZD7288. Right: summary graph of change in firing rates caused by LTG, in the absence and presence of ZD7288, as a function of injected current. (**c**) Left: LTP at SC-CA1 synapses is impaired in vehicle-treated slices from *Nf1*$^{9a-/9a-}$ mice ($n = 9$) compared with WT mice ($n = 6$, $P < 0.01$). Right: LTG rescues the LTP deficit in *Nf1*$^{9a-/9a-}$ mice ($n = 10$ and $n = 16$ for WT and *Nf1*$^{9a-/9a-}$, respectively, P

= 0.2). (**d**) LTG rescues the learning deficits in $Nf1^{9a-/9a-}$ mice in a water maze probe trial, (two-way analysis of variance (ANOVA), genotype × drug interaction, $F_{1,43} = 6.0$, $P < 0.05$). The black and white columns represent the target quadrant (TQ) and average time spent in other quadrants, respectively. Although vehicle-treated $Nf1^{9a-/9a-}$ mice ($n = 9$) spend only 27% of their time in the TQ, LTG-treated $Nf1^{9a-/9a-}$ mice ($n = 12$) show 45% TQ preference ($P < 0.05$). LTG has no significant effect on spatial learning in WT mice (vehicle, $n = 12$ and LTG, $n = 14$, $P = 0.3$). (**e**) LTG rescues the spatial learning deficits of $Nf1^{+/-}$ mutants (two-way ANOVA, genotype × drug interaction, $F_{1,40} = 5.2$, $P < 0.05$). Vehicle-treated $Nf1^{+/-}$ mice show no preference for the TQ (25%, $n = 9$), whereas LTG-treated $Nf1^{+/-}$ mice show robust learning (44%, $n = 10$; $P < 0.05$). LTG has no significant effect on WT mice (Vehicle, $n = 13$, and LTG, $n = 12$; $P = 0.4$). The heatplots are visual representation of all search tracks, in which the color indicates the mean time spent at a certain position. Statistical analyses were performed by Student's *t*-test and two-way ANOVA followed by Tukey's test. $^*P < 0.05$. Data represent the mean ± s.e.m.